Fano Resonances in Plasmonic Nanoparticle Aggregates[†]

Nikolay A. Mirin,[‡,§,∥] Kui Bao,[‡,§,⊥] and Peter Nordlander*[,§,⊥]

Laboratory for Nanophotonics and Department of Chemistry, MS 60, Rice University, Houston, Texas 77005-1892, and Department of Physics, MS 61, Rice University, Houston, Texas 77005-1892

Received: November 26, 2008; Revised Manuscript Received: January 13, 2009

We investigate the plasmonic properties of a symmetric silver sphere septamer and show that the extinction spectrum exhibits a narrow Fano resonance. Using the plasmon hybridization approach and group theory we show that this Fano resonance is caused by the interference of two bonding dipolar subradiant and superradiant plasmon modes of E_{1u} symmetry. We investigate the effect of structural symmetry breaking and show that the energy and shape of the Fano resonance can be tuned over a broad wavelength range. We show that the wavelength of the Fano resonance depends very sensitively on the dielectric permittivity of the surrounding media with one of the highest LSPR sensitivities reported for a finite nanostructure.

I. Introduction

Plasmonic nanostructures are of considerable current interest because of many important applications in chemical sensing and biosensing,[1−3] subwavelength waveguiding,[4−6] metamaterial applications,[7−9] imaging and fluorescence applications,[10−12] and biotechnology.[13−15] The unique ability of plasmons to focus incident light into subwavelength volumes near metal surfaces can lead to very intense local fields.[16] The field intensities of such hotspots can reach sufficient levels to enable single molecule Surface Enhanced Raman Scattering (SERS).[17] The largest plasmonic field enhancements are typically occurring in junctions between adjacent nanoparticles. For this reason much experimental and theoretical effort has been devoted to the study of the plasmonic properties of nanoaggregates such as dimers,[18−22] trimers and quadrumers,[23−26] and larger structures such as nanoparticle chains and arrays.[27−32]

The line widths of plasmon resonances play a crucial role in many applications. In SERS applications the maximum obtainable field enhancements generally become larger for narrower resonances. In waveguiding application, the propagation length is typically proportional to the plasmon lifetime. In Localized Surface Plasmon Resonance (LSPR) sensing where analytes are detected through their screening-induced shift of the energy of a plasmon resonance, the efficiency of a plasmonic substrate is typically determined by the Figure of Merit (FoM) defined as the shift of the energy of the plasmon resonance per refractive unit of surrounding material divided by the width of the resonance.[33] In LSPR sensing applications it is therefore crucial to employ substrates with narrow plasmon resonances.

The plasmon line width is determined by both intrinsic and radiative damping. The intrinsic damping is proportional to the imaginary part of the dielectric function and depends on both the material and the wavelength. By employing tunable plasmonic nanoparticles such as nanorods or nanoshells, and tuning the plasmon resonance to a wavelength longer than the onset for interband transitions, the intrinsic damping can be reduced. The radiative damping depends on the total dipole moment of the plasmon resonance. The total dipole moment associated with a collective plasmon mode in a multiparticle aggregate depends on the relative phase of the dipolar plasmon modes of the individual particles. If the individual nanoparticle dipoles oscillate in phase, the plasmon mode is superradiant and strongly radiative. In subradiant modes the dipoles oscillate out of phase, resulting in a drastic reduction of the radiative damping. A dramatic example of the effect of radiative damping has been demonstrated in a concentric ring-disk cavity, i.e., a planar disk concentrically aligned within a planar ring.[34] In this system the dipolar modes of the disk and rings interact and form hybridized bonding and antibonding plasmon modes. The low-energy bonding mode is subradiant and extremely narrow while the antibonding mode is superradiant and appears like a broad continuum.

The interference between subradiant and superradiant plasmon modes can result in narrow Fano resonances in the optical spectrum of a nanostructure.[8,35−37] Apart from their fundamental importance, such Fano resonances are also of considerable interest in LSPR sensing application because of the large FoM that can be achieved for narrow resonances. For instance, for a nonconcentric aligned ring-disk cavity,[35] the FoM of the Fano resonance is larger than 8, which is among the largest FoM reported for a standalone nanostructure.

In a recent study of the plasmonic properties of nanoshell arrays we showed that a symmetric Au nanoshell septamer can exhibit a pronounced Fano resonance in the infrared part of the spectrum.[38] In this paper we investigate the microscopic mechanism that provides this interference effect by an application to a smaller symmetric Ag nanosphere septamer. We show that the septamer geometry with its unique symmetry properties is particularly amenable to exhibit Fano resonances. According to group theory, the irreducible representation of the symmetric septamer is the sum of the representation for the center particle (CP) and that of the surrounding six particle ring hexamer (HX). Thus two types of dipolar resonances are formed in this structure, hybridized bonding and antibonding linear combinations of the HX and CP modes. The Fano resonance results from the interference of a narrow subradiant bonding mode of E_{1u} symmetry, which overlaps another broad bonding superradiant mode of the same symmetry. The Fano resonance of the

[†] Part of the "George C. Schatz Festschrift".
* Corresponding author. E-mail: nordland@rice.edu.
[‡] These authors contributed equally to the project.
[§] Laboratory for Nanophotonics.
[∥] Department of Chemistry.
[⊥] Department of Physics.

10.1021/jp810411q CCC: $40.75
Published on Web 02/17/2009

septamer is found to exhibit a very large LSPR sensitivity with a FoM above 10.

The organization of the paper is as follows. In Section II we calculate the optical spectra of the septamer and use group theory to analyze the nature of the plasmon modes. In Section III we investigate the microscopic nature of the Fano resonance. Finally, in Section IV, we analyze the effect of structural symmetry breaking and the LSPR sensitivity of the septamer.

II. Plasmonic Structure of a Septamer

A number of theoretical methods have been developed for the calculation of the optical properties of nanostructures.[39−41] In this paper we will use the Finite-Difference Time-Domain method (FDTD),[42] a commercial implementation COMSOL of the Finite Element Method (FEM), and the Plasmon Hybridization (PH) approach.[43] The PH method is an electrostatic approach that expresses the plasmon resonances of a composite nanostructure in terms of the plasmonic modes of the individual constituent nanoparticles. In the present calculation, we include all primitive nanosphere plasmons up to an $l_{max} = 20$. which is sufficient for convergence.

The metallic particles in this study are assumed to be silver spheres. Normally the Ag metal will be modeled by using experimental dielectric data (JC).[44] To make it easier to resolve individual plasmon modes in the spectra in some instances we will also employ a Drude Fit (DF) where the dielectric function is parametrized as,

$$\epsilon_{DF} = \epsilon_\infty + \frac{{\omega_B}^2}{\omega(\omega - i\delta)} \quad (1)$$

with $\omega_B = 9.1721$ eV, $\epsilon_\infty = 4.039$, and $\delta = 0.0207$ eV. This parametrization provides a reasonable fit of the JC data for wavelengths larger than 400 nm. In the electrostatic limit (PH), this parametrization corresponds to sphere multipolar plasmon energies

$$\omega_l = \omega_B \sqrt{\frac{l}{(\epsilon_\infty + 1)l + 1}} \quad (2)$$

To describe the geometry of a symmetric septamer consisting of spherical particles of radius R and nearest neighbor separation d we introduce the notation (R,d). All spectra will be calculated assuming normal incidence. As for a symmetric trimer and quadrumer,[23] one can use group theory to show that the symmetric septamer spectra is independent of the in-plane polarization angle.

In Figure 1 we show the different cross sections of a symmetric (50,5) nm septamer. The extinction and scattering spectra reveal several narrow features. Unless defined explicitly scattering means the electromagnetic energy scattered by a structure from the incident beam integrated over 4π solid angle. The most prominent resonance is the Fano antiresonance around 570 nm. This feature is robust and appears for symmetric septamers of $R = 50$ nm Ag spheres for interparticle spacings d in the range 2 to 10 nm and probably beyond. The antiresonance at 570 nm is analogous to the Fano resonance discussed for a much larger symmetric nanoshell septamer.[38]

A. Plasmon Modes of the Septamer. In Figure 2 we show the plasmon resonances of the septamer as a function of interparticle spacing calculated using the PH approach. For the largest separation, the interaction between the plasmon modes of different nanoparticles is very small and the plasmon modes are essentially the $7(2l + 1)$ degenerate modes of the individual nanosphere plasmon ω_l. As the separation d is decreased, the

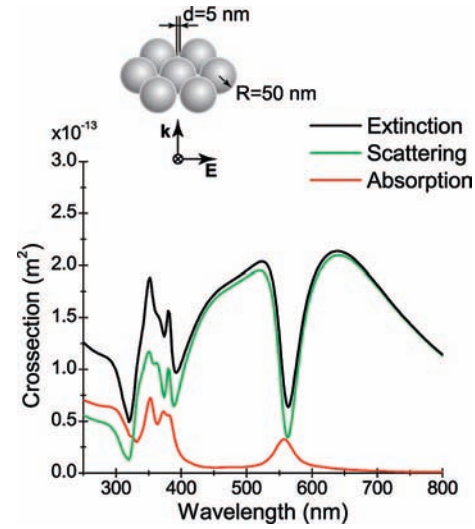

Figure 1. Extinction (black), scattering (green), and absorption (red) cross sections of a symmetric (50,5) nm Ag septamer calculated for normal incidence, using JC dielectric data.

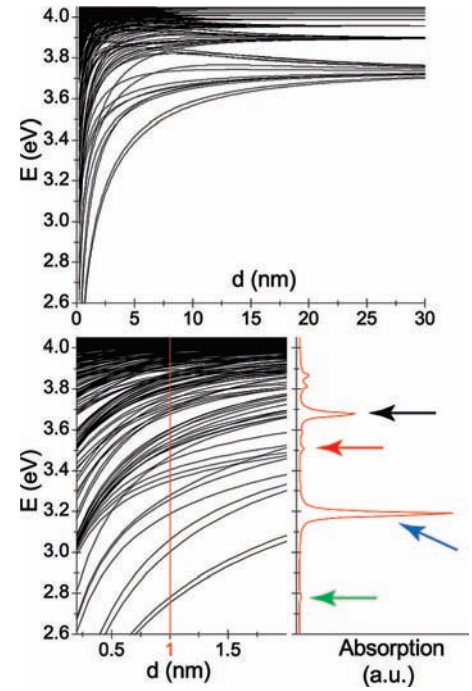

Figure 2. Energy (upper and lower left panels) of the plasmon resonances in a (10,d) nm symmetric silver septamer calculated as a function of d. The bottom right panel shows the absorption spectra for the $d = 1$ nm structure. The arrows denote some of the dipole active modes. The silver metal is modeled by using the DF parametrization. Only plasmon resonances in the energy interval 2.6 to 4.1 eV are shown.

modes begin to interact and hybridized collective septamer plasmon modes are formed. The lowest group of levels are the bonding and antibonding modes that asymptotically originate from the dipolar modes. At slightly larger energies, the highly degenerate quadrupolar mode forms a less dispersive manifold of hybridized plasmon modes. Quadrupolar and the higher multipolar resonance interacts very weakly. As the separation is further decreased also modes of different multipolar index l begin to interact resulting in asymmetric splittings of the bonding and antibonding levels. This interaction also results in higher modes becoming dipole active and being able to couple to incident light. This is apparent in the absorption spectrum for d

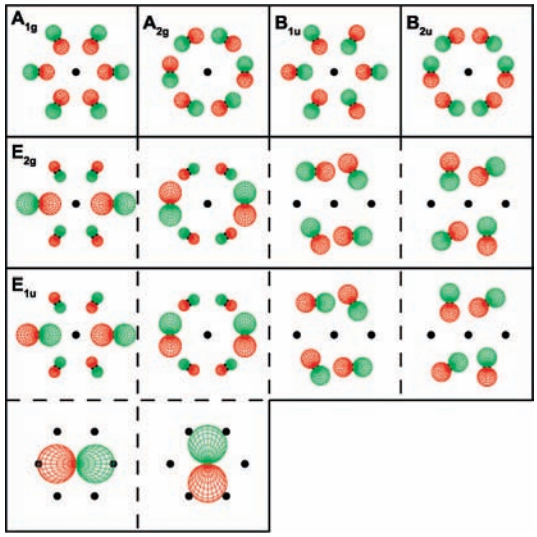

Figure 3. Symmetry adapted basis functions of septamer planar dipoles generated by using the D_{6h} point group. Only the E_{1u} panels contain modes with finite dipole moments.

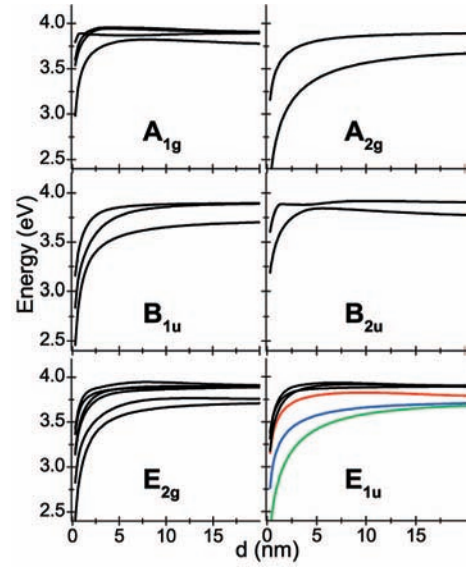

Figure 4. Symmetry resolved plasmon frequencies of the (10,*d*) nm septamer as a function of *d* calculated with PH. The silver metal is modeled by using the DF parametrization. The colored curves of E_{1u} correspond to the features in the absorption spectrum in Figure 2.

= 10 nm, which shows two strong features at 3.5 and 3.7 eV which originate from the $l = 1$ nanosphere modes but also several weak features originating from hybridized $l = 2$ modes.

B. Group Theoretical Analysis. The PH approach allows for a very simple interpretation of the plasmonic structure using group theory.[23,24] The present application to the septamer closely parallels the previously published application to symmetric trimers and quadrumers.[23]

The septamer geometry belongs to the D_{6h} point group, and contains two distinct particle types with respect to the symmetry operations. The CP is located at the intersection of all symmetry elements and it is independent from the six peripheral particles that are connected to each other with group symmetry operators. The septamer symmetry-adapted basis set is thus the union of that for the HX and that for an isolated sphere. The irreducible representation of the septamer can thus be written as $\Gamma_{\text{Sept}} = \Gamma_{\text{CP}} + \Gamma_{\text{HX}}$, where the irreducible representations for the planar dipole modes of the sphere and the HX are,

$$\Gamma_{\text{CP}} = 2E_{1u}$$
$$\Gamma_{\text{HX}} = A_{1g} + A_{2g} + B_{1u} + B_{2u} + 4E_{2g} + 4E_{1u}$$

This decoupling of the symmetry adapted basis for the septamer into a symmetry adapted basis for the HX and the CP is responsible for the unique plasmonic properties of the septamer.

For the septamer there are 21 individual dipolar plasmon modes. We will consider only in-plane modes and assume that the incident *E*-field is always in the plane of our structure. The 14 individual in-plane dipolar modes transform into 14 symmetry adapted basis functions as illustrated in Figure 3. In a dipole representation the CP contributes only to the E_{1u} representation. The E_{1u} representation exhibits a 6-fold degeneracy and the physical plasmon modes are constructed as linear combinations of all 6 E_{1u} basis modes. The CP dipolar plasmon can thus hybridize with the surrounding ring dipolar modes and form bonding and antibonding modes as well as dark subradiant and bright superradiant modes.

With use of the symmetry adapted basis function (Figure 3), the individual septamer plasmon modes in Figure 2 can be classified by irreducible representation. In Figure 4, we show the lowest plasmon modes within each symmetry group as a function of interparticle separation *d*. The figure shows that for decreasing *d* the plasmon energies at Figure 4 decrease. This red-shift is a specific effect observed for the septamer geometry and not observed in smaller systems such as the dimer, trimer, or quadrumer. For example, the dipole modes of A_{1g} symmetry depicted in Figure 3 suggest a strong electrostatic repulsion that results in these modes being antibonding in a HX structure. However, in the septamer this repulsion is countered by an attractive interaction mediated by multipolar plasmons of the CP, which results in an effective attractive interaction and red-shift at small *d*. Another effect specific to the septamer geometry is the avoided crossings of plasmon modes, which emerges as a result of the interaction between the CP and the peripheral particles. This effect is responsible for the energy overlap of the subradiant and superradiant modes. The coloring of the E_{1u} modes in Figure 4 corresponds to the color of the arrows denoting the peaks in the absorption spectrum in Figure 2.

III. Analysis of the Septamer Fano Resonance

In this section, we analyze the microscopic origin of the Fano resonance in the extinction spectrum (Figure 1) for the (50,5) nm septamer.

Fano resonances in plasmonic systems can be intuitively understood by using a coupled damped harmonic oscillator model originally developed as a classical analogy to Electromagnetically Induced Transparency (EIT) in atomic systems.[45] Fano resonances appear naturally in such systems when narrow dark modes couple to and spectrally overlap broad bright modes. The effective interaction between the two such modes is dispersive and can result in a strong interference in the oscillator amplitudes which in turn influence the radiation emitted from the system, i.e. the scattering spectrum. When the two oscillator modes are of similar frequency the interference results in a symmetric antiresonance. If the frequencies are different, the typical asymmetric Fano resonance appears. The PH method directly expresses plasmons in composite nanoparticles as coupled damped harmonic oscillators. Dark plasmons with little or no dipole moments are narrow, and bright plasmons with sizable dipole moments are superradiant and strongly damped. The interaction between plasmon modes on adjacent nanoparticles is controlled by the geometry of the structure.

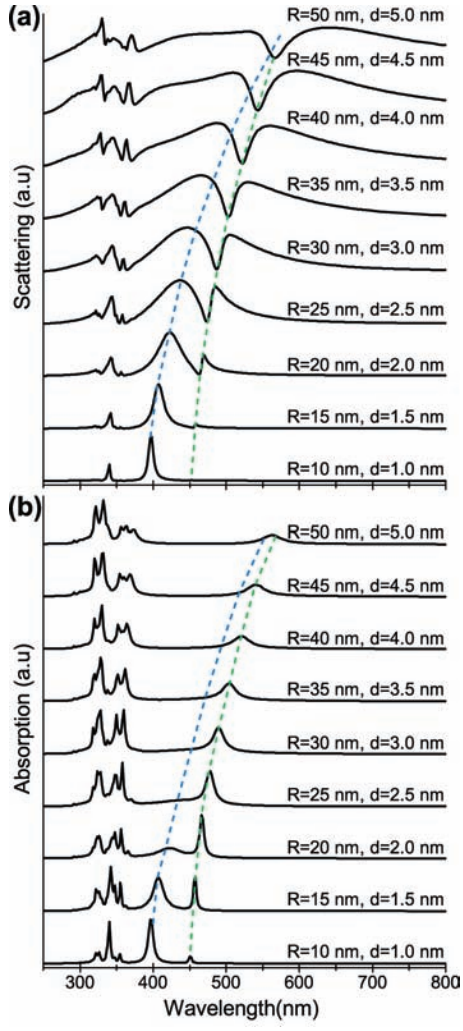

Figure 5. Scattering (a) and absorption (b) spectra calculated with FEM of the septamer as a function of overall size of the system. The Ag is modeled by using the DF dielectric parametrization. The dashed curves show the red-shift of the subradiant (green) and superradiant (blue) modes with increasing size.

In Figure 5 we show the scattering and absorption spectra for the septamer with all dimensions scaled down by a common factor. For the smallest system (10,1) nm, the scattering and radiative damping is very small and the absorption spectrum agrees perfectly with the result from the electrostatic PH approach shown in Figure 2. The two strong features at 340 and 380 nm are the two bonding E_{1u} modes (black and blue lines in Figure 4). The very weak feature at 450 nm is the almost dark bonding subradiant E_{1u} (green line in Figure 4) with the dipole moment of the center atom oriented opposite to the dipole moment of the surrounding six ring atoms. The nature of this mode will be discussed in detail below.

As the size of the system is increased, scattering becomes more important than absorption. The superradiant E_{1u} mode begins to red-shift and broadens significantly while the dark mode remains narrow and red-shifts only weakly. For $R > 25$ nm, the superradiant mode is sufficiently broad to overlap the dark mode. When this happens, the conditions for radiative plasmonic interference effects are satisfied. The dispersive coupling between the narrow subradiant mode and the broad continuum of the superradiant mode results in an asymmetric Fano resonance at the energy of the subradiant mode. For $R =$ 50 nm, the energies of the subradiant and superradiant modes

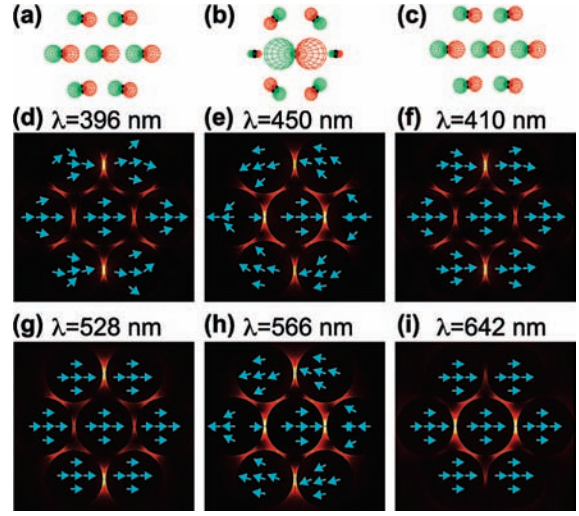

Figure 6. Electric field direction (blue arrows) and enhancement (color contour with red and yellow indicating hot spots) associated with the subradiant (center column) and on the blue (left column) and red (right column) sides of the superradiant septamer plasmon modes. Panels a−c show the dipolar admixtures calculated with PH. Panels d−f are for the (10,1) nm septamer and panels g−i are for the (50,5) nm septamer. The maximum field enhancements for the (50,5) nm septamer are 53, 88, and 43 at 528, 566, and 642 nm wavelengths.

are approximately equal and a characteristic antiresonance appears in the spectra.

The absorption spectra in Figure 5b illustrate the dramatic effect radiation damping has on the line width of bright plasmon resonances in finite systems of increasing size. For R larger than 25 nm, the superradiant mode is not discernible in the absorption spectrum. The reason for that is that the mode radiates much more strongly than it absorbs. Although the mode still exhibit a finite albeit small absorption, the intensity is too small to result in a Fano resonance in the absorption spectra.

In Figure 6 we show the electric field enhancements of the subradiant and superradiant modes for the (10,1) nm septamer calculated using PH. This small septamer is in the quasistatic regime, so FEM and PH both give the same results. We also show the field enhancements for three wavelengths around the Fano resonance for the (50,5) nm septamer where retardation effects play a dominant role. These plots are very similar to the result for the electrostatic (10,1) nm system where a group theoretical analysis can be rigorously justified. The dipolar components of the modes calculated with PH are shown in Figure 6a−c and clearly show that both the subradiant and superradiant modes are different bonding linear combinations of the symmetry-adapted basis functions depicted in the E_{1u} panel of Figure 3. For the superradiant mode, the dipolar mode of the CP oscillates with the same phase as the dipolar plasmons in the surrounding ring and therefore exhibit significant broadening due to radiation damping. For the subradiant state, the dipole moment of the CP is opposite to the dipole moments of the ring plasmons. Thus the total dipole moment is reduced and the width of the resonance is determined by the intrinsic damping.

Since the symmetry properties of the septamer are such that the plasmon modes can be regarded as having been formed through hybridization of the modes of the CP and those of the surrounding HX, it is of interest to investigate the effect of changing the radius of the CP. Such a change does not break the symmetry of the septamer. In Figure 7a, we show the extinction spectra of the (50,5) nm septamer when substituting the CP with a sphere of different radius R_C. For the smallest R_C

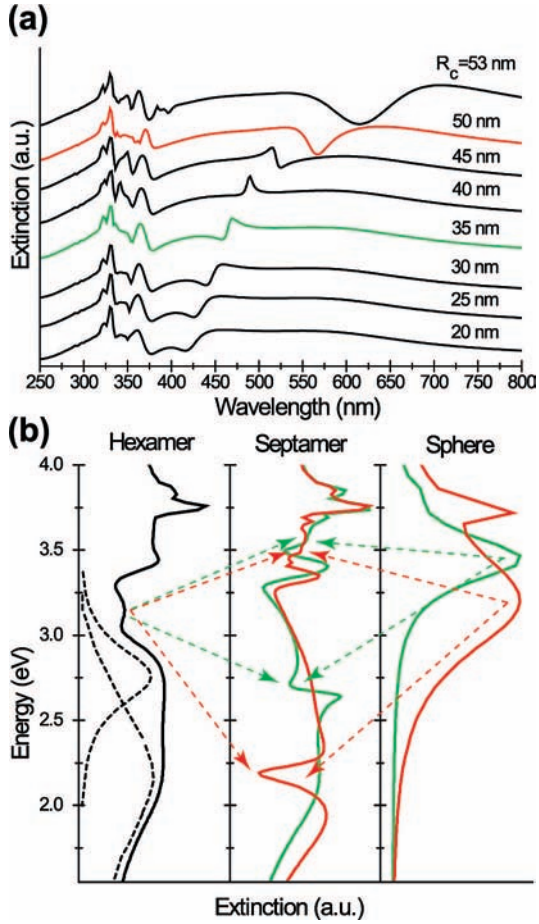

Figure 7. (a) Effect of replacing the CP in a (50,5) nm septamer by a sphere of different radius $R_C = 35$ nm (red) and 50 nm (green). (b) A PH hybridization diagram showing how the bonding subradiant septamer mode (center) is formed from the interaction of the HX (left) and the CP (right). The two dashed lines in the HX are two different and overlapping superradiant HX states. The arrows represent the interactions between the relevant states.

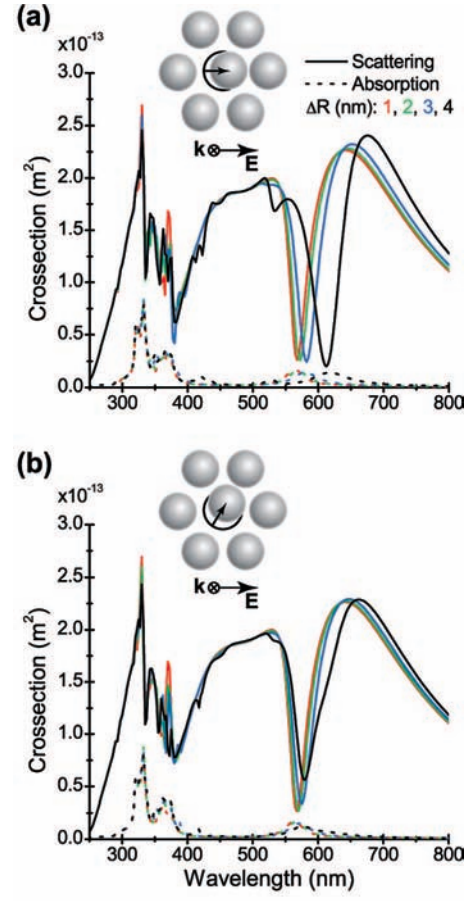

Figure 8. Effect of a lateral displacement of the CP on the extinction spectrum of the (50,5) nm septamer: (a) Displacement in the direction of the polarization of the incident light. (b) Displacement at a 60° angle with respect to the polarization of the incident light.

= 20 nm, the interaction between the CP and the surrounding HX is negligible and the spectrum is essentially a superposition of the spectra for a (50,5) nm HX and the spectrum of a silver nanosphere of radius 20 nm. The plasmonic structure of the HX will be analyzed in detail elsewhere. Briefly, the optically active modes are linear combinations of the first four basis functions of E_{1u} symmetry depicted in Figure 3. The HX modes that are relevant in the present discussion include a relatively narrow mode around 400 nm and a continuum extending between 425 and 800 nm that is made up of two superradiant modes centered around 450 and 600 nm. The 400 nm mode interacts with the CP dipole to form the hybridized bonding subradiant mode depicted in Figure 6b. This mode is highly tunable with a wavelength that depends strongly on R_C. As the radius R_C becomes larger, the interaction between the CP plasmons and ring plasmons increases and interference effects begin to play a role. For $R_C = 35$ nm, the subradiant mode begins to interfere with the short wavelength edge of the HX continuum resulting in a characteristic asymmetric Fano resonance at 450 nm. As R_C increases, the interaction increases resulting in a further red-shift of the subradiant state into the HX continuum and a change of the line shape of the Fano resonance. For the largest $R_C = 50$ and 53 nm, the Fano resonance appears as an antiresonance in the lower energy HX continuum.

In Figure 7b we illustrate schematically how the plasmon resonances of the CP and the surrounding HX hybridize to form the subradiant state that results in the Fano resonance. To make the PH more apparent the extinction spectra are plotted as a function of energy rather than wavelength. The figure clearly shows how the dipolar nanosphere plasmon interacts with a HX mode around 3.2 eV and forms a bonding subradiant mode in the HX continuum. For $R_C = 35$ nm, the subradiant state is red-shifted to around 2.7 eV, where it appears as an asymmetric Fano resonance. For $R_C = 50$ nm, the state is further red-shifted to 2.2 eV and appears in the spectrum as an antiresonance.

IV. Discussion

Realistic plasmonic systems always deviate from ideal models and it is crucial to understand the most important variations that may affect the system properties. Some variations such as symmetry breaking may even result in new important physical effects or improve the properties of the system. In the first subsections we investigate how robust the Fano resonance is to slight distortions, i.e., symmetry breaking of the septamer geometry. In the second subsection we investigate the LSPR sensitivity of the septamer Fano resonance and show that it is remarkably large.

A. Symmetry Breaking. Planar nanoparticle assemblies are most commonly fabricated on flat substrates, which makes the lateral particle positions difficult to control with high accuracy.[46,47]

In Figure 8 we investigate the effect of symmetry breaking on the extinction spectrum of the (50,5) nm septamer. When

the symmetry of the septamer is broken, the extinction spectrum will no longer be independent of the in-plane polarization angle. To maximize the effect we consider only CP displacements directly toward one of the surrounding HX nanoparticles. Such a displacement represents the largest change in interparticle spacings and therefore the largest change of the CP−HX interactions. For simplicity we consider a lateral displacement of the CP in two different directions with respect to the polarization of incident light. In Figure 8a we show the effect of a CP displacement along the direction of incident polarization. The figure shows a clear red-shift of the subradiant Fano resonance due to the increased interaction between the CP plasmon and the surrounding ring. For the largest displacement, a new Fano resonance appears around 550 nm. For the displacement of the CP in a direction at a 60° angle with respect to the polarization vector, the effect is smaller but still induces a clearly discernible red-shift of the Fano resonance. For both displacements, however, the Fano resonance remains clearly visible in the extinction spectrum. If the symmetry of the system is disturbed significantly Fano resonance may still appear for specific spatial orientations and incident beam polarizations.

Fano resonances are expected to occur very generally in asymmetric nanoparticle aggregates when their overall size is sufficiently large for a superradiant mode to broaden sufficiently to provide a background continuum. If a dark mode with dispersive coupling exists within this continuum, the condition for EIT is satisfied and a Fano resonance will appear.[45] In a recent study of the plasmonic properties of random nanoparticle aggregates, the authors show highly polarization dependent extinction spectra for a pentamer consisting of five nanoparticles of various sizes in a nonsymmetrical configuration.[48] The spectra are very complex with multiple peaks and antipeaks which most likely are Fano resonances resulting from the interference of subradiant and superradiant modes.

We would expect Fano resonances also to occur for a symmetric hexamer consisting of a center particle surrounded by a symmetric five-membered nanoparticle ring or larger structures of D_{6h} symmetry such as septamers surrounded by one or several outer rings. However, for a strong Fano antiresonance to appear, it is crucial that the bonding mode is subradiant, i.e., has a very small dipole moment. The symmetry properties of the septamer are quite unique in that the bonding mode is dark because its parent modes, the center particle dipole, and the surrounding hexamer dipole have similar dipole moments thus resulting in a dark hybridized bonding mode. It is interesting to note that the concentric ring-disk cavity, which for a small disk and large thin ring can be viewed as a center particle surrounded by a large number of small disks, does not display a Fano resonance.[34] The reason is that the dipole moment of the ring is much larger than the dipole moment of the disk thus resulting in hybridized modes of similar dipole moments.

B. LSPR Sensing. Plasmonic interference and coherence effects such as Fano resonances are caused by plasmon−plasmon interactions and can therefore be very strongly affected by the electrostatic screening introduced by the presence of dielectric media between adjacent nanoparticles.[35] The septamer Fano resonance with its distinct and narrow shape in the visible region of the spectrum thus provides an interesting candidate as an efficient LSPR sensor. In Figure 9 we show the extinction spectra of a septamer placed on a glass substrate surrounded by dielectric embedding media of different permittivities. Figure 9a shows the effect of only filling the junctions with the embedding media and Figure 9b shows the effect of completely covering the septamer structure. Both panels demonstrate that

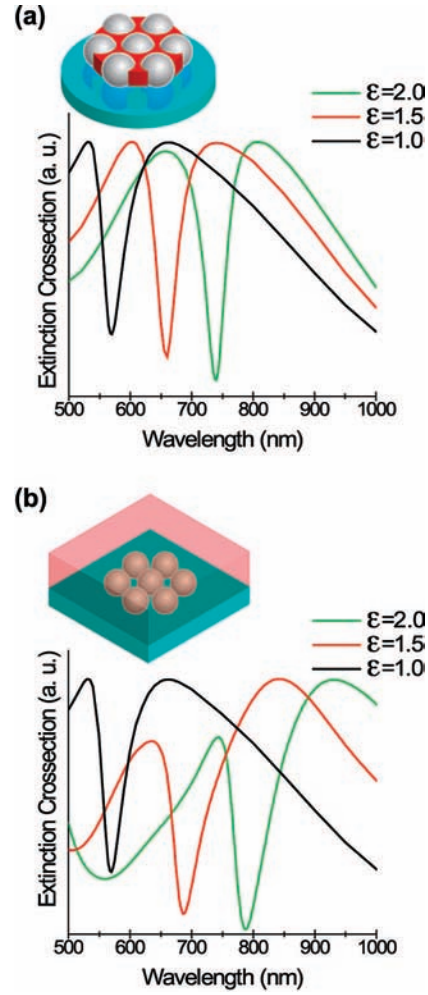

Figure 9. Effect of partially (a) and completely (b) surrounding a (50,5) nm septamer by dielectric media on the extinction spectrum. The permittivities are 1.0 (black), 1.5 (red), and 2.0 (green). The septamer is placed on a glass substrate of permittivity 2.09. The metal is modeled by using JC. The shape of the dielectric insertions is indicated in the insets.

the effect of dielectric screening is a strong red-shift of the Fano resonance. The LSPR shift for the Fano resonance in Figure 9a is 410 nm/RIU and for a complete embedding of the septamer as shown in Figure 9b, the LSPR shift is 515 nm/RIU. The full width half-maximum of the Fano resonance defined as the energy difference between the peak on the short wavelength side of the antiresonance and the energy of its minimum is 0.15 eV. The corresponding FoM are thus 7.9 and 10.6, which shows that the septamer structure would provide an excellent platform for LSPR sensing.

The plasmonic interference effects responsible for the large LSPR sensitivity originate from the particular symmetry properties of a septamer and are likely to arise also for septamers consisting of cylindrical disks which may be readily fabricated by using lithographic techniques.

V. Conclusion

Using numerical and analytical electromagnetic methods we have analyzed the optical and plasmonic properties of symmetric Ag nanosphere septamers. The unique symmetry of a septamer leads to a decoupling of its plasmon modes into plasmon modes of the six surrounding ring particles and the plasmon modes of the center particle. The interaction between the plasmon modes

of the center particle with the plasmon modes of the surrounding ring results in hybridized bonding and antibonding septamer plasmon. The interference between a bonding subradiant and a bonding superradiant septamer plasmon results in a pronounced Fano resonance in the extinction spectrum. This Fano resonance is found to be well preserved also for a weak structural symmetry breaking of the septamer. The Fano resonance is found to exhibit an unusually large LSPR sensitivity making the septamer structure a highly promising substrate for LSPR sensing.

Acknowledgment. This material is based upon work supported by, or in part by, the U.S. Army Research Laboratory and the U.S. Army Research Office under contract/grant number W911NF-04-1-0203, the Robert A. Welch Foundation under grant C-1222, and the National Science Foundation under grant CNS-0421109.

References and Notes

(1) Lal, S.; Grady, N. K.; Kundu, J.; Levin, C. S.; Lassiter, J. B.; Halas, N. J. *Chem. Soc. Rev.* **2008**, *37*, 898–911.
(2) Pelton, M.; Aizpurua, J.; Bryant, G. W. *Laser Photon. Rev.* **2008**, *2*, 136–159.
(3) Ko, H.; Singamaneni, S.; Tsukruk, V. V. *Small* **2008**, *4*, 1576–1599.
(4) Lal, S.; Link, S.; Halas, N. J. *Nature Phot.* **2007**, *1*, 641–648.
(5) Oulton, R. F.; Sorger, V. J.; Genov, D. A.; Pile, D. F. P.; Zhang, X. *Nature Phot.* **2008**, *2*, 496–500.
(6) Maier, S. A. *Nature Phot.* **2008**, *2*, 460–461.
(7) Korobkin, D.; Urzumov, Y. A.; Neuner, B.; Norman, C.; Zhang, Z.; Mayergoyz, I. D.; Shvets, G. *Appl. Phys. A: Mater. Sci. Process.* **2007**, *88*, 605–609.
(8) Christ, A.; Martin, O. J. F.; Ekinci, Y.; Gippius, N. A.; Tikhodeev, S. G. *Nano Lett.* **2008**, *8*, 2171–2175.
(9) Liu, N. A.; Fu, L.; Kaiser, S.; Schweizer, H.; Giessen, H. *Adv. Mater.* **2008**, *20*, 3859–3865.
(10) Tam, F.; Goodrich, G. P.; Johnson, B. R.; Halas, N. J. *Nano Lett.* **2007**, *7*, 496–501.
(11) Fleischer, M.; Stanciu, C.; Stade, F.; Stadler, J.; Braun, K.; Heeren, A.; Haffner, M.; Kern, D.; Meixner, A. J. *Appl. Phys. Lett.* **2008**, *93*, 111114.
(12) Grosges, T.; Barchiesi, D.; Toury, T.; Grehan, G. *Opt. Lett.* **2008**, *33*, 2812–2814.
(13) Liu, C. H.; Mi, C. C.; Li, B. Q. *IEEE Trans. Nanobiosci.* **2008**, *7*, 206–214.
(14) Zhang, J.; Fu, Y.; Chowdury, M. H.; Lakowicz, J. R. *J. Phys. Chem. C* **2008**, *112*, 9172–9180.
(15) Khlebtsov, N. G. *Quantum Electron.* **2008**, *38*, 504–529.
(16) Qin, L.; Zou, S.; Xue, C.; Atkinson, A.; Schatz, G. C.; Mirkin, C. A. *Proc. Natl. Acad. Sci. U.S.A.* **2006**, *103*, 13300–13303.
(17) Ward, D. R.; Halas, N. J.; Ciszek, J. W.; Tour, J. M.; Wu, Y. P.; Nordlander, P.; Natelson, D. *Nano Lett.* **2008**, *8*, 919–924.
(18) Yim, T.-J.; Wang, Y.; Zhang, X. *Nanotechnology* **2008**, *19*, 435605.
(19) Wei, H.; Hakansson, U.; Yang, Z.; Hook, F.; Xu, H. X. *Small* **2008**, *4*, 1296–1300.
(20) Hossain, M. K.; Kitahama, Y.; Huang, G. G.; Kaneko, T.; Ozaki, Y. *Appl. Phys. B: Laser Opt.* **2004**, *93*, 165–170.
(21) Hartling, T.; Alaverdyan, Y.; Hille, A.; Wenzel, M. T.; Kall, M.; Eng, L. M. *Opt. Express* **2008**, *16*, 12362–12371.
(22) Giannini, V.; Sanchez-Gil, J. A. *Opt. Lett.* **2008**, *33*, 899–901.
(23) Brandl, D. W.; Mirin, N. A.; Nordlander, P. *J. Phys. Chem. B* **2006**, *110*, 12302–12310.
(24) Urzhumov, Y. A.; Shvets, G.; Fan, J.; Capasso, F.; Brandl, D. W.; Nordlander, P. *Opt. Express* **2007**, *15*, 14129–14145.
(25) Alegret, J.; Rindzevicius, T.; Pakizeh, T.; Alaverdyan, Y.; Gunnarsson, L.; Kall, M. *J. Phys. Chem. C* **2008**, *112*, 14313–14317.
(26) Xu, S. P.; Hartvickson, S.; Zhao, J. X. J. *Langmuir* **2008**, *24*, 7492–7499.
(27) Hicks, E. M.; Zou, S.; Schatz, G. C.; Spears, K. G.; van Duyne, R. P.; Gunnarsson, L.; Rindzevicius, T.; Kasemo, B.; Kall, M. *Nano Lett.* **2005**, *5*, 1065–1070.
(28) Kim, P.-Y.; Lee, D. H.; Kim, S. J.; Jang, D.-J. *J. Colloid Inteface Sci.* **2008**, *326*, 3897–391.
(29) Pinchuk, A. O.; Schatz, G. C. *Appl. Phys. B: Laser Opt.* **2008**, *93*, 31–38.
(30) Hossain, M. K.; Shimada, T.; Kitajima, M.; Imura, K.; Okamoto, H. *Langmuir* **2008**, *24*, 9241–9244.
(31) Luo, W.; van der Veer, W.; Chu, P.; Mills, D. L.; Penner, R. M.; Hemminger, J. C. *J. Phys. Chem. C* **2008**, *112*, 11609–11613.
(32) Liu, C. H.; Hong, M. H.; Cheung, H. W.; Zhang, F.; Huang, Z. Q.; Tan, L. S.; Hor, T. S. A. *Opt. Express* **2008**, *16*, 10701–10709.
(33) Sherry, L. J.; Chang, S. H.; Schatz, G. C.; van Duyne, R. P.; Wiley, B. J.; Xia, Y. *Nano Lett.* **2005**, *5*, 2034–2038.
(34) Hao, F.; Nordlander, P.; Burnett, M. T.; Maier, S. A. *Phys. Rev. B* **2007**, *76*, 245417.
(35) Hao, F.; Sonnefraud, Y.; Dorpe, P. V.; Maier, S. A.; Halas, N. J.; Nordlander, P. *Nano Lett.* **2008**, *8*, 3983–3988.
(36) Zhang, S.; Genov, D. A.; Wang, Y.; Liu, M.; Zhang, X. *Phys. Rev. Lett.* **2008**, *101*, 047401.
(37) Bachelier, G.; Russier-Antoine, I.; Benichou, E.; Jonin, C.; Fatti, N. D.; Vallee, F.; Brevet, P.-F. *Phys. Rev. Lett.* **2008**, *101*, 197401.
(38) Le, F.; Brandl, D. W.; Urzhumov, Y. A.; Wang, H.; Kundu, J.; Halas, N. J.; Aizpurua, J.; Nordlander, P. *ACS Nano* **2008**, *2*, 707–718.
(39) Myroshnychenko, V.; Rodrigues-Fernandez, J.; Pastoriza-Santos, I.; Funston, A. M.; Novo, C.; Mulvaney, P.; Liz-Marzan, L. M.; de Abajo, F. J. G. *Chem. Soc. Rev.* **2008**, *37*, 1792–1805.
(40) Montgomery, J. M.; Lee, T. W.; Gray, S. K. *J. Phys.: Condens. Matter* **2008**, *20*, 323201.
(41) Zhao, J.; Pinchuk, A. O.; McMahon, J. M.; Li, S.; Ausman, L. K.; Atkinson, A. L.; Schatz, G. C. *Acc. Chem. Res.* **2008**, *41*, 1710–1720.
(42) Oubre, C.; Nordlander, P. *J. Phys. Chem. B* **2004**, *108*, 17740–17747.
(43) Prodan, E.; Nordlander, P. *J. Chem. Phys.* **2004**, *120*, 5444–5454.
(44) Johnson, P. B.; Christy, R. W. *Phys. Rev. B* **1972**, *6*, 4370–4379.
(45) Alzar, C. L. G.; Martinez, M. A. G.; Nussenzveig, P. *Am. J. Phys.* **2002**, *70*, 37–41.
(46) Khanal, B. P.; Zubarev, E. R. *Angew. Chem., Int. Ed.* **2007**, *46*, 2195–2198.
(47) Mirin, N. A.; Hainey, M.; Halas, N. J. *Adv. Mater.* **2008**, *20*, 535–538.
(48) Xu, H.; Kall, M. *Top. Appl. Phys.* **2006**, *103*, 86–103.

JP810411Q